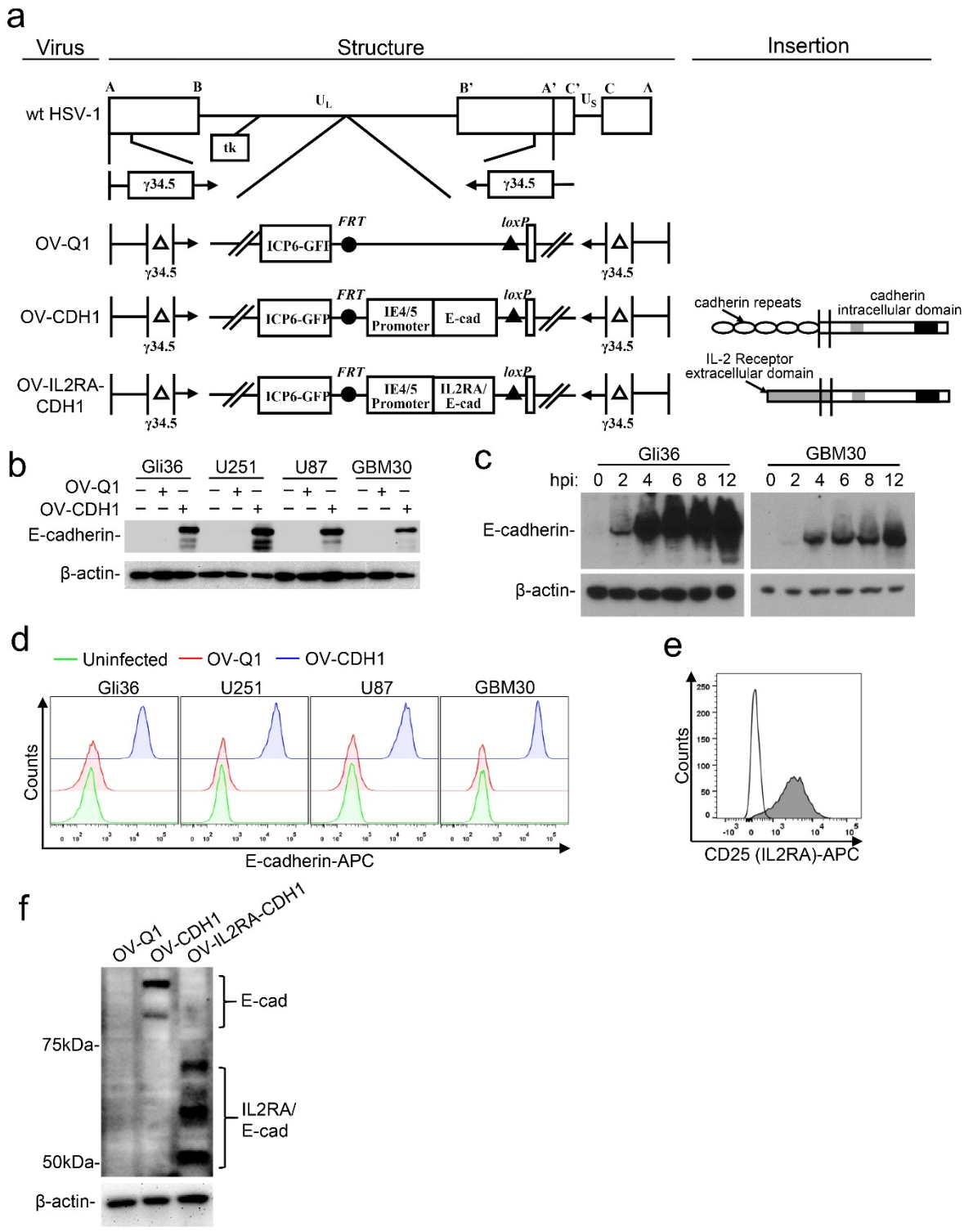

Supplementary Figure 1. The constructions and biological characteristics of OV-Q1, OV-CDH1 and OV-IL2RA-CDH1. (**a**) Schematic map of oncolytic viruses used in this study. Top: genetic map of wild type HSV-1. Second: genetic map of control oHSV, OV-Q1, with deletion of γ34.5, dysfunction of ICP6, and insertion of the GFP gene. Third: genetic map of OV-CDH1 showing the insertion of the human *CDH1* gene (encoding E-cad) driven by the viral pIE4/5 promoter. Fourth: The genetic maps of OV-IL2RA-CDH1 demonstrating the insertion of protein-

coding sequence of mutant E-cad (IL2RA/E-cad), in which the original E-cad extracellular domain was replaced with the interleukin-2 receptor alpha chain (IL2RA) extracellular domain, while cytoplasmic domain remained intact. (**b**) Immunoblotting performed with cell lysates from uninfected, OV-Q1- or OV-CDH1-infected Gli36, U251, U87 and GBM30 cells at 8 hpi. (**c**) Immunoblotting performed with lysates from OV-CDH1-infected Gli36 or GBM30 cells at 0, 2, 4, 6, 8, 12 hpi. (**d**) E-cad surface expression was determined by flow cytometry on uninfected, OV-Q1- or OV-CDH1-infected GBM cells at 8 hpi. (**e**) Determinination of IL2RA/E-cad surface expression by flow cytometry on OV-IL2RA-CDH1-infected U251 cells at 8 hpi using an anti-CD25 antibody. The experiments in (**b**-**e**) were repeated 3 times with similar results. (**f**) Immunoblotting performed with cell lysates from OV-Q1-, OV-CDH1- and OV-IL2RA-CDH1-infected U251 cells at 8 hpi using an antibody recognizing the cytoplasmic domain of E-cad. The experiment was repeated twice with similar results.

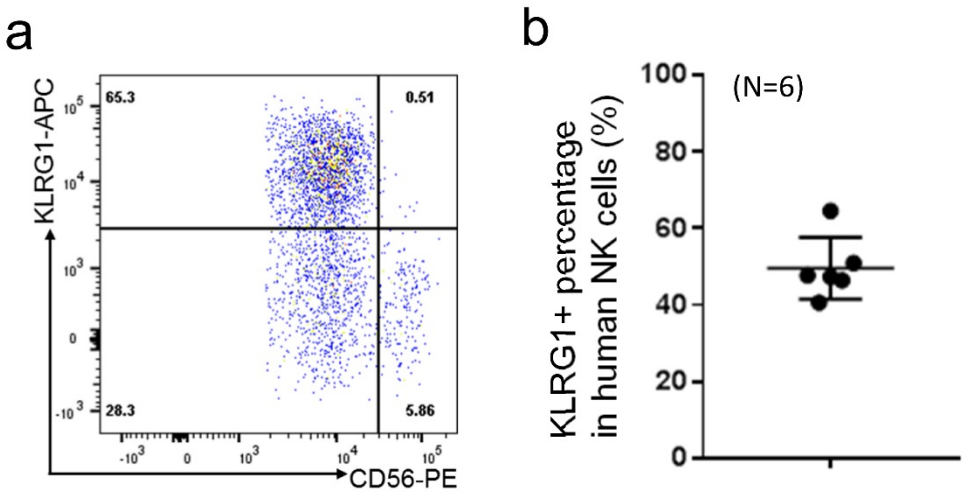

Supplementary Figure 2. KLRG1 expression in human NK cells. (**a**) Freshly isolated human NK cells were stained with anti-KLRG1-APC and anti-CD56-PE antibodies and analyzed with flow cytometry. A representative flow cytometric plot is presented (n = 6 donors). (**b**) The proportions of KLRG1^{+} NK cells among total NK cells in the peripheral blood assessed in 6 different healthy donors. Data are presented as mean ± SD.

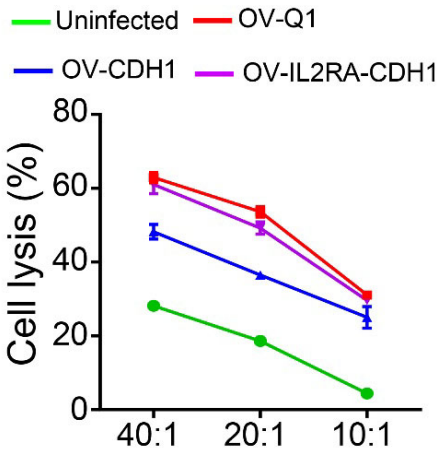

Supplementary Figure 3. Replacement of E-cadherin extracellular domain diminishes the inhibitory effect of E-cadherin on NK cell cytotoxicity. Cytotoxicity levels of freshly isolated human primary NK cells were measured by ^{51}Cr release assays. Target cells were uninfected, OV-Q1-, OV-CDH1- and OV-IL2RA-CDH1-infected Gli36 and the effector:target ratios were 40:1, 20:1 and 10:1. This experiment was repeated 3 times with NK cells isolated from different donors with similar results.

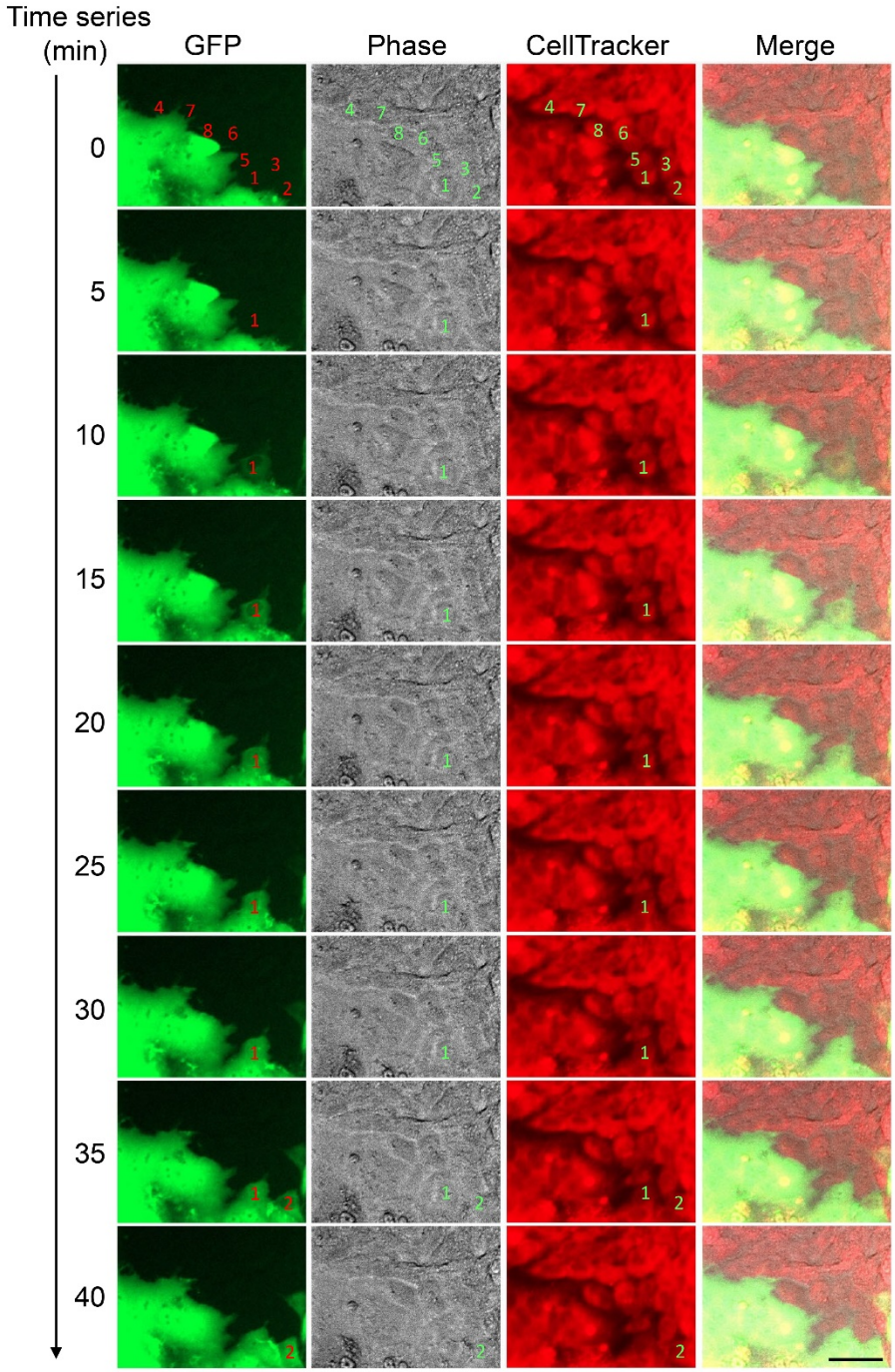

Supplementary Figure 4. Time-lapse (0~40 min) fluorescence and phase images of the cell-cell fusion process during OV-CDH1 infection. The dynamic change of OV-CDH1-infected cells and the surrounding uninfected cells was recorded by a series of time-lapse fluorescence and phase images. The time interval between every two rows was 5 min. Green fluorescence (GFP) indicates the infected cells; Red fluorescence indicates the cytoplasmic content of all the cells stained with CellTracker; Phase images show the cell morphology and the membrane structure. Eight uninfected cells surrounding the infected cells were labeled with numbers (1 to 8) in the figure. Figure 3 shows that the first 2 uninfected cells successively fused into the OV-CDH1-infected cells along with the cell membranes fusing, new syncytia forming and cytoplasmic content sharing processes. Scale bar, 50 μm. This experiment was repeated 5 times with similar results.

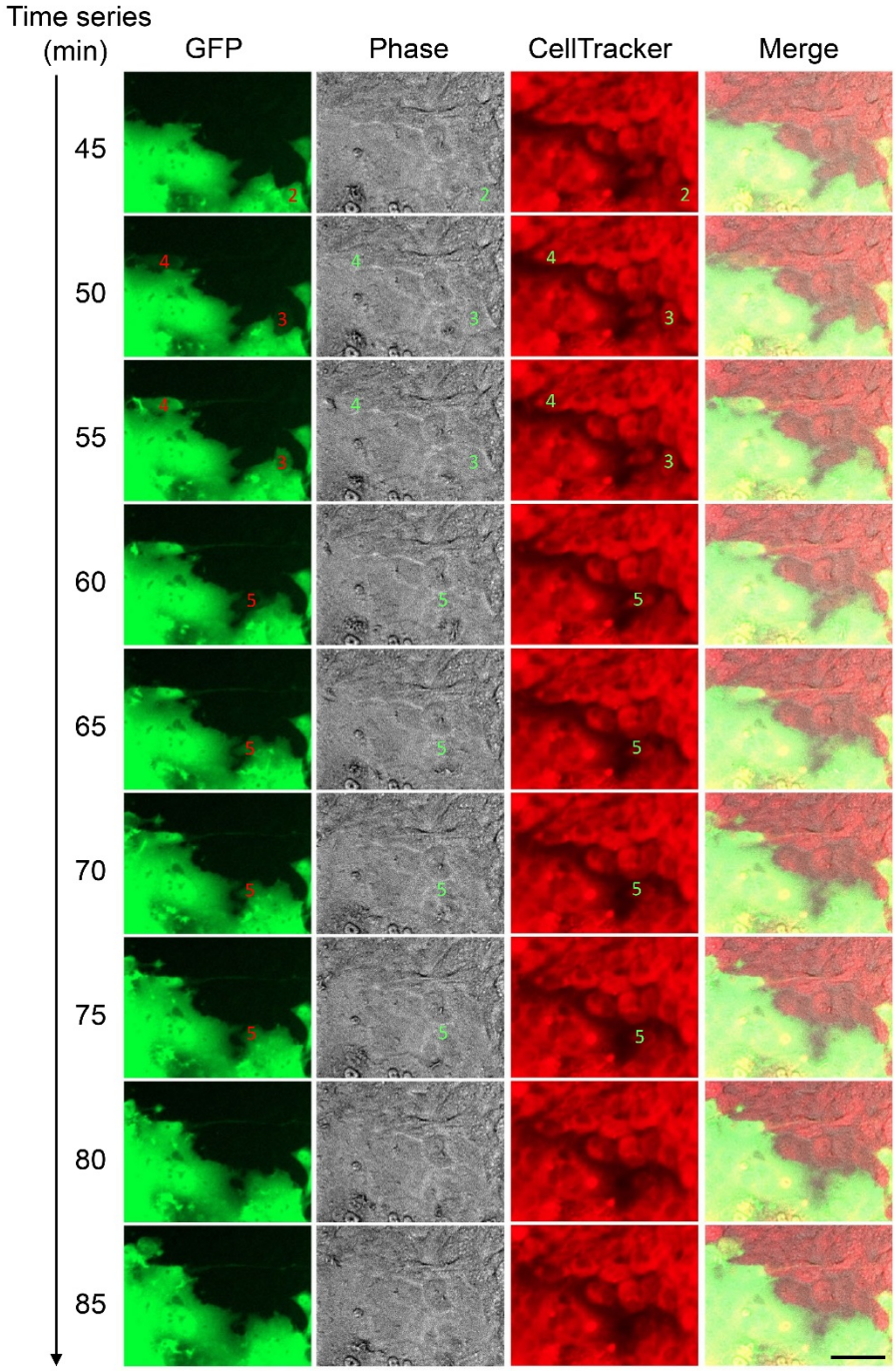

Supplementary Figure 5. Time-lapse (45~85 min) fluorescence and phase images of the cell-cell fusion process during OV-CDH1 infection. The images in this figure were taken followed those in Supplementary Figure 3. The dynamic change of OV-CDH1-infected cells and the surrounding uninfected cells was recorded by a series of time-lapse fluorescence and phase images. The time interval between every two rows was 5 min. Green fluorescence (GFP) indicates the infected cells; Red fluorescence indicates the cytoplasmic content of all the cells stained with CellTracker; Phase images show the cell morphology and the membrane structure. Eight uninfected cells surrounding the infected cells were labeled with numbers (1 to 8) in the figure. Figure 4 shows that uninfected cells (2 to 5) successively fused into the OV-CDH1-infected cells along with the cell membranes fusing, new syncytia forming and cytoplasmic content sharing processes. Scale bar, 50 μm. This experiment was repeated 5 times with similar results.

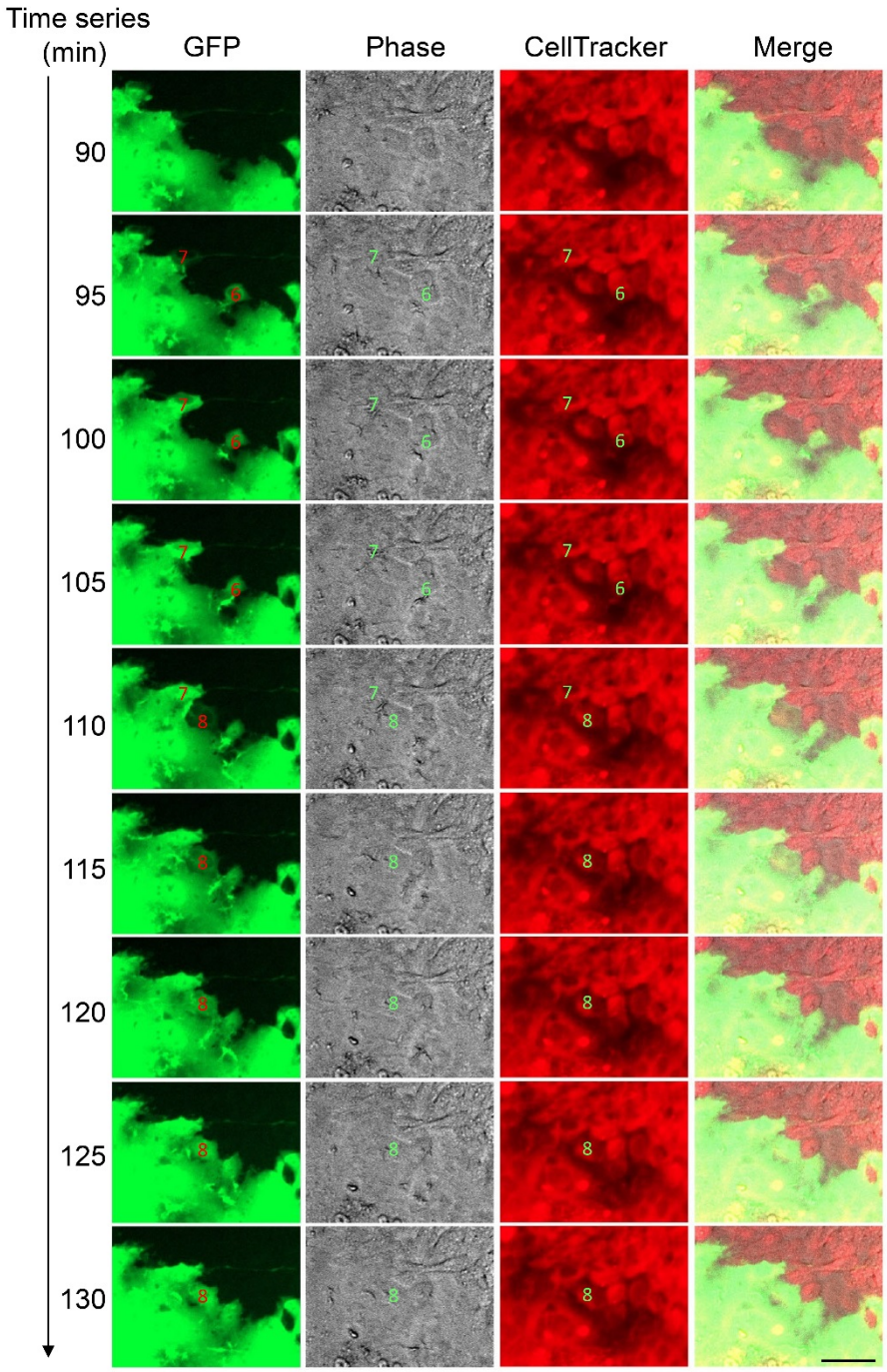

Supplementary Figure 6. Time-lapse (90~130 min) fluorescence and phase images of the cell-cell fusion process during OV-CDH1 infection. The images in this figure were taken followed those in Supplementary Figure 4. The dynamic change of OV-CDH1-infected cells and the surrounding uninfected cells was recorded by a series of time-lapse fluorescence and phase images. The time interval between every two rows was 5 min. Green fluorescence (GFP) indicates the infected cells; Red fluorescence indicates the cytoplasmic content of all the cells stained with CellTracker; Phase images show the cell morphology and the membrane structure. Eight uninfected cells surrounding the infected cells were labeled with numbers (1 to 8) in the figure. Figure 5 shows that uninfected cells (6 to 8) successively fused into the OV-CDH1-infected cells along with the cell membranes fusing, new syncytia forming and cytoplasmic content sharing processes. Scale bar, 50 μm. This experiment was repeated 5 times with similar results.

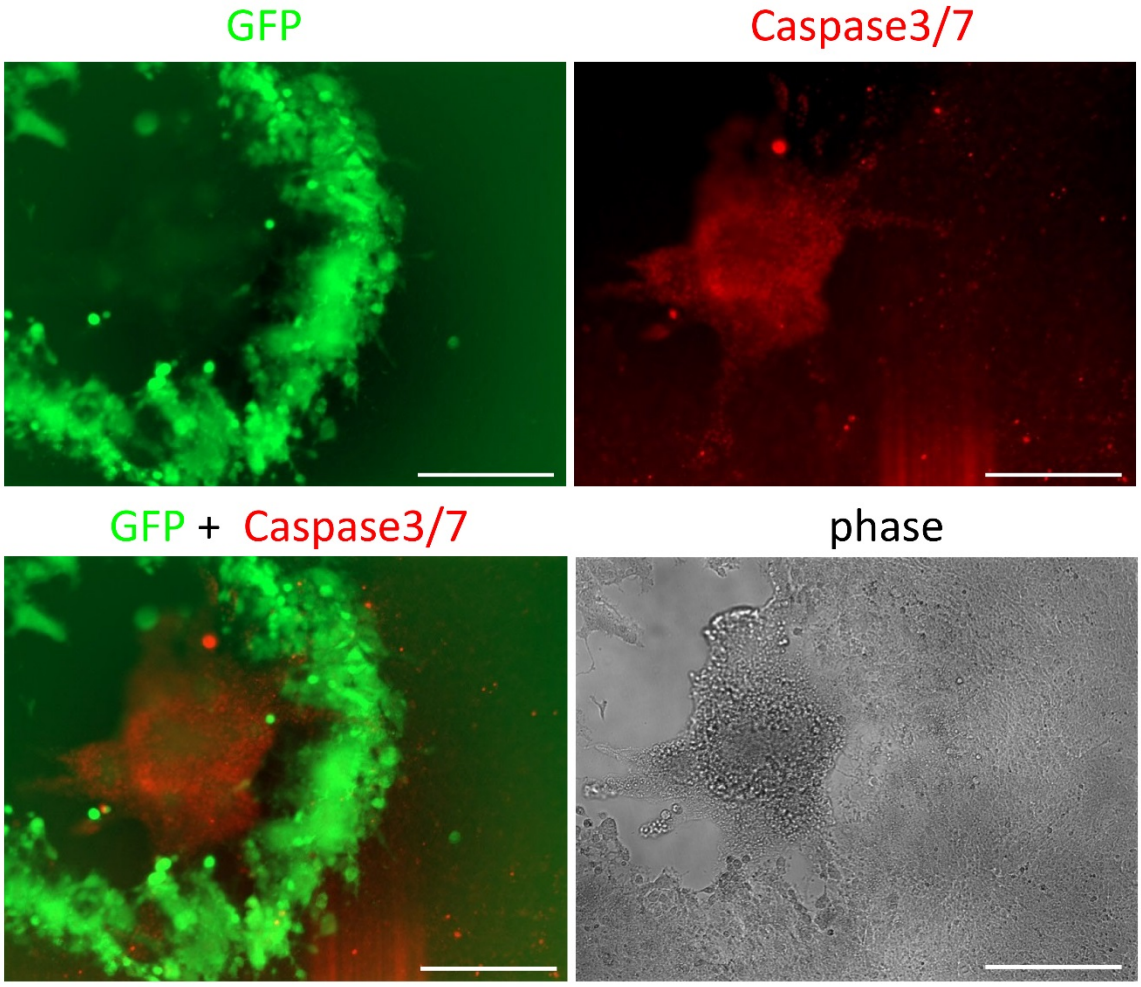

Supplementary Figure 7. Caspase-3/7 staining of OV-CDH1-infected U251 cells. OV-CDH1-infected U251 cells were stained with Caspase-3/7 fluorescence dye and imaged at 48 hpi with a microscope. Green fluorescence (GFP) indicates the OV-CDH1-infected cells. Red fluorescence indicates Caspase 3/7 positive staining. Scale bar, 150 μm. This experiment was repeated 3 times with similar results.

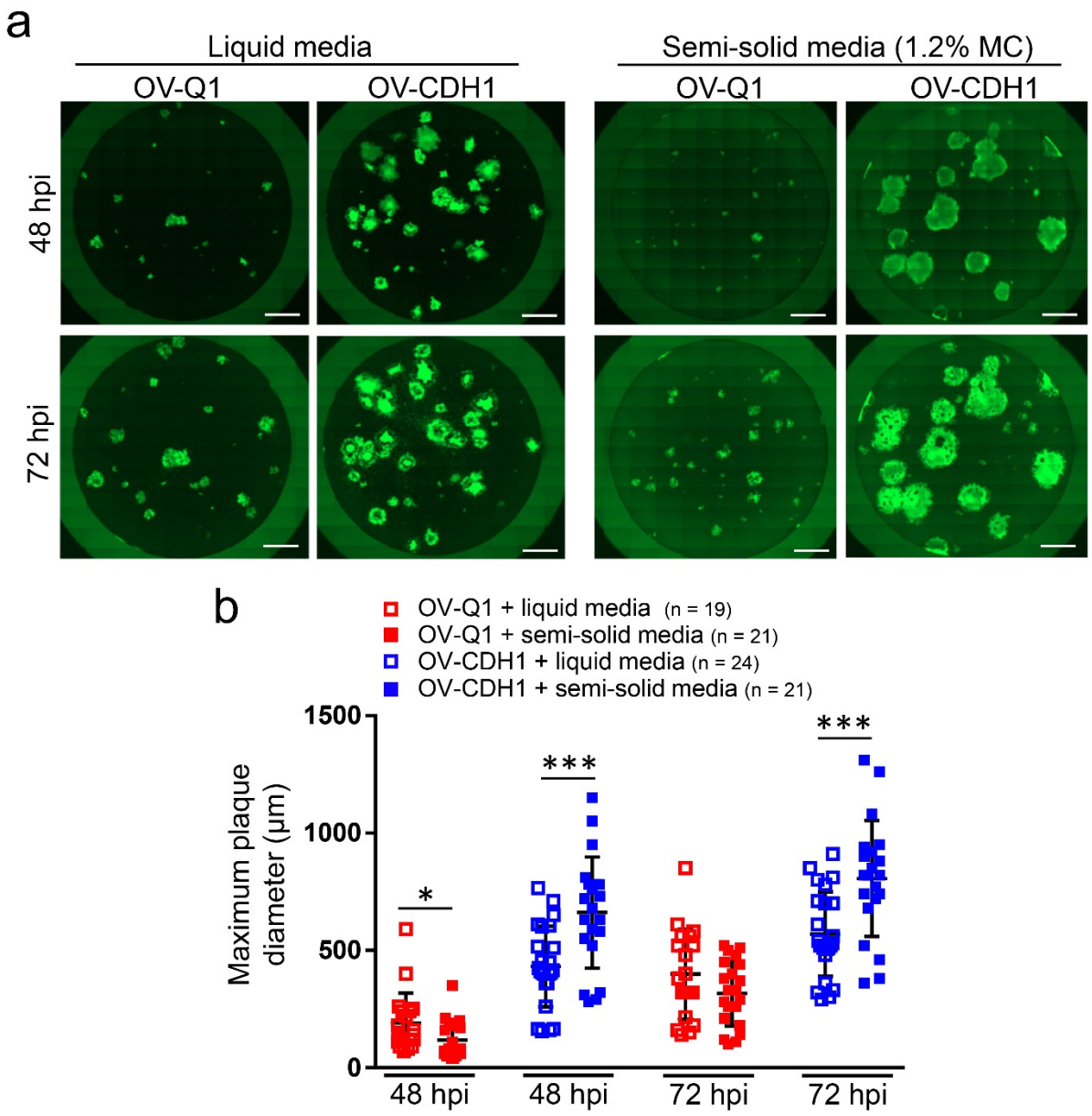

Supplementary Figure 8. Plaque forming assay with liquid and semi-solid media. (**a**) Intratumoral viral spread environment was mimicked with semi-solid media containing 1.2% methylcellulose. Monolayer U251 cells in 96-well plates were infected with OV-Q1 and OV-CDH. At 2 hpi, infection media were replaced with fresh or semi-solid media containing 1.2% methylcellulose. Cells were then imaged at 48 and 72 hpi with a microscope. Scale bar, 1,000 µm. This experiment was performed with 3 technical replicates. (**b**) Quantification of plaque diameter in (**a**). Data are presented as mean ± SD. For OV-Q1 at 48 hpi, liquid media vs. semi-solid media $*P = 0.034$. For OV-CDH1 at 48 hpi, liquid media vs. semi-solid media $***P < 0.001$. For OV-CDH1 at 72 hpi, liquid media vs. semi-solid media $***P < 0.001$. *P* values were generated by unpaired two-tailed *t*-test. Sample sizes are indicated in the figures. This experiment was repeated 3 times with similar results.

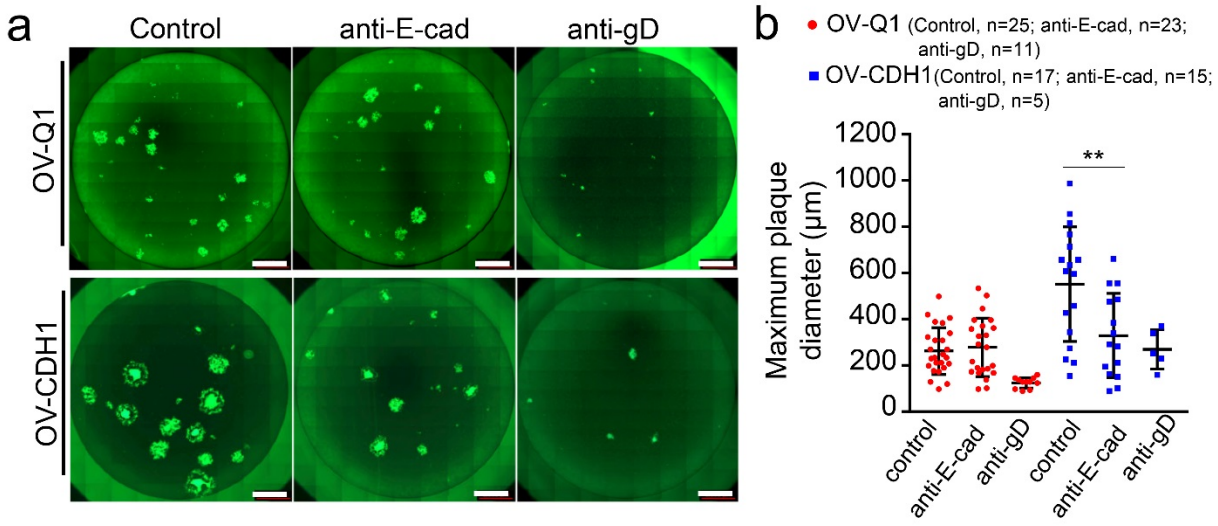

Supplementary Figure 9. E-cad blockade with a neutralizing antibody lowers the enhancement of viral spread by OV-CDH1. (**a**) Monolayer Gli36 cells in 96-well plates were infected with OV-Q1 or OV-CDH1 at a MOI of 0.005. At 2 hpi, infection media were replaced with media containing an E-cad blocking antibody or isotype control (rat IgG1κ). gD blocking antibody was used as positive control. Cells were imaged with a microscope at 48 hpi. Scale bar, 1,000 μm. (**b**) Quantification of plaque diameter in (a). Data are presented as mean ± SD. Unpaired two-tailed *t*-test was used to compare the control and anti-E-cad groups. Control vs. anti-E-cad $^{**}P = 0.008$. Sample sizes are indicated in the figures. This experiment was repeated 3 times with similar results.

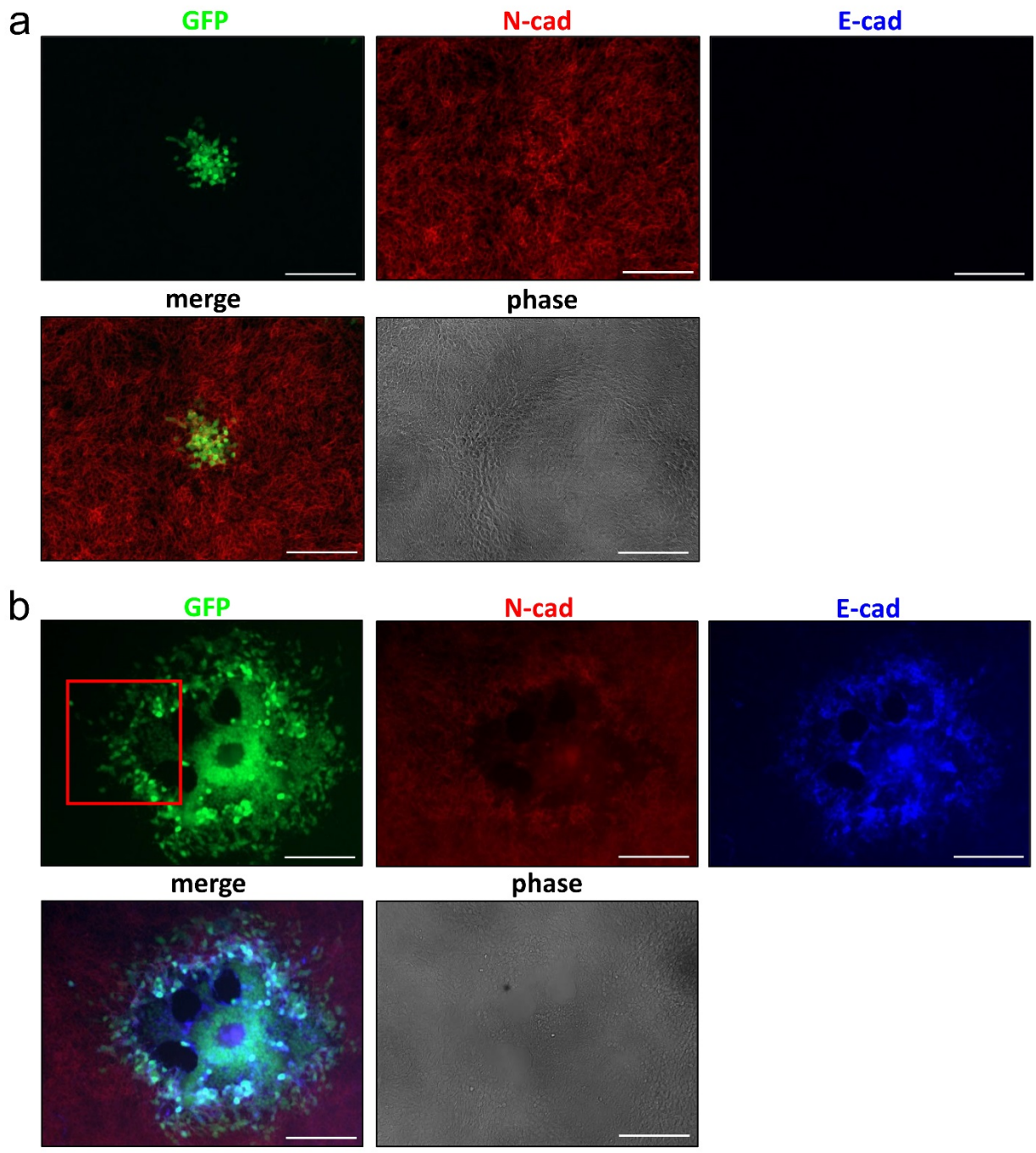

Supplementary Figure 10. Co-localization of human E-cad and human N-cad in OV-CDH1-infected human GBM cells. U251 cells were infected with OV-Q1 (**a**) or OV-CDH1 (**b**). immunofluorescence staining was performed with the infected cells using anti-E-cad and anti-N-cad antibodies at 48 hpi. Cells were then imaged using a microscope. The red square indicates the location of the images shown in Figure 3c. Scale bar, 150 μm. This experiment was repeated 5 times with similar results.

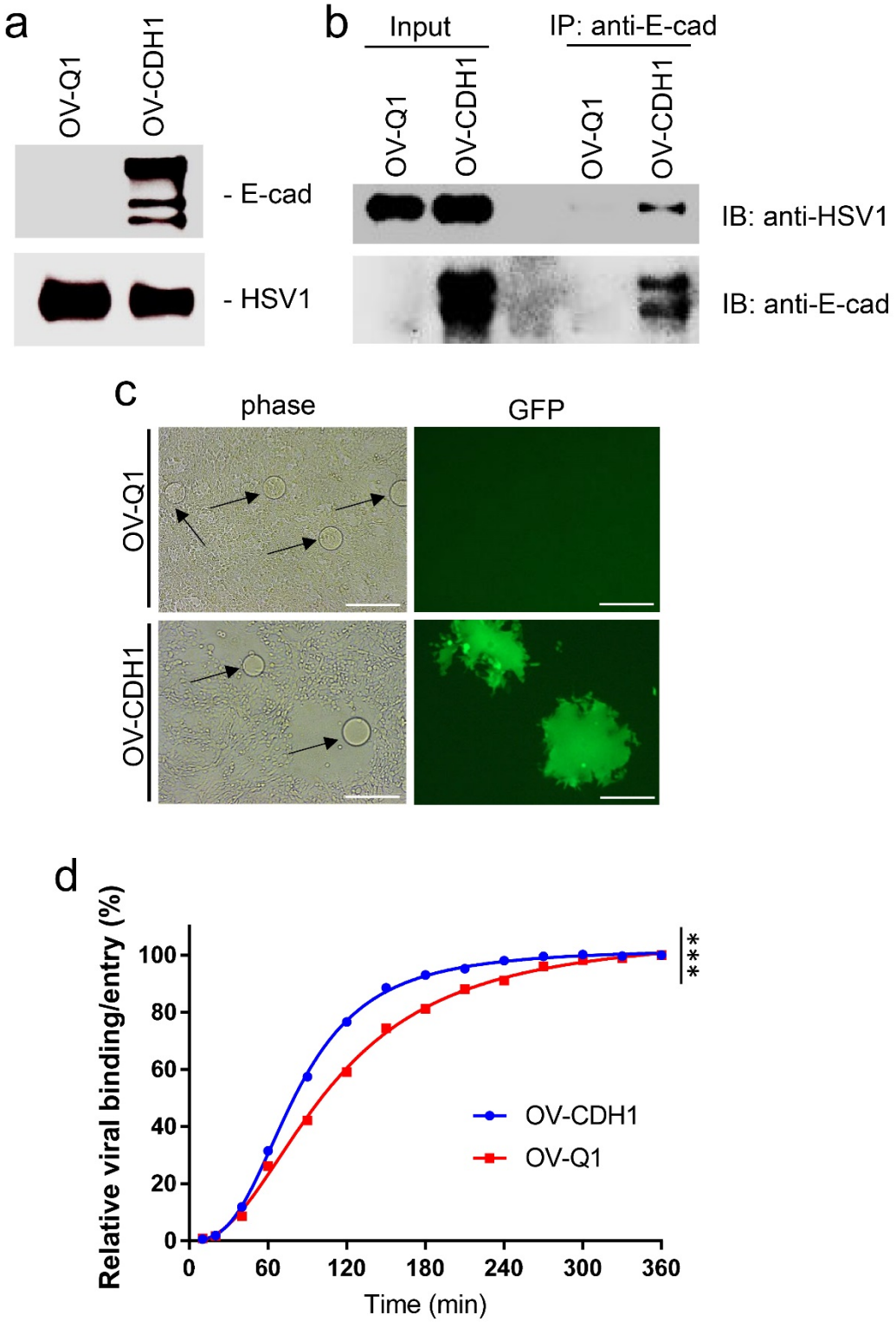

Supplementary Figure 11. Viral membrane loaded E-cad may accelerate viral entry. (**a**) Immunoblot of E-cad incorporation in purified OV-Q1 or OV-CDH1 virus particles. (**b**) Immunoprecipitation (IP) assay with purified viral particles. Anti-E-cad-coated agarose beads were incubated with purified OV-CDH1 or OV-Q1 particles for 1 hour followed by 9 washes. The pull-down lysates were detected by immunoblotting for E-cad and HSV. (**c**) Agarose beads (pointed by arrows) from (**b**) were added to monolayer Gli36 cells. Cells were imaged with a

fluorescent microscope 48 hours after adding the beads. Scale bar, 250 μm. The experiments in (**a-c**) were repeated 3 times with similar results. (**d**) Flow cytometry-based viral binding/entry kinetics. Viral particles of OV-CDH1 and OV-Q1 were labeled with fluorescence lipophilic dye DiD. Gli36 cells were infected with DiD-labeled viruses and washed with PBS at various time points following infection (10 to 360 min) to remove the unbound viral particles. Cells with virus bound or entered were determined by flow cytometry. The viral binding/entry vs. time curves were established to evaluate viral binding/entry kinetics. Nonlinear models were fitted for each treatment group over time by Generalized Additive Model (R package "mgcv") and F test was used to compare the residual sum of squares which resulted in a P value of < 0.001. This experiment was repeated 3 times with similar results.

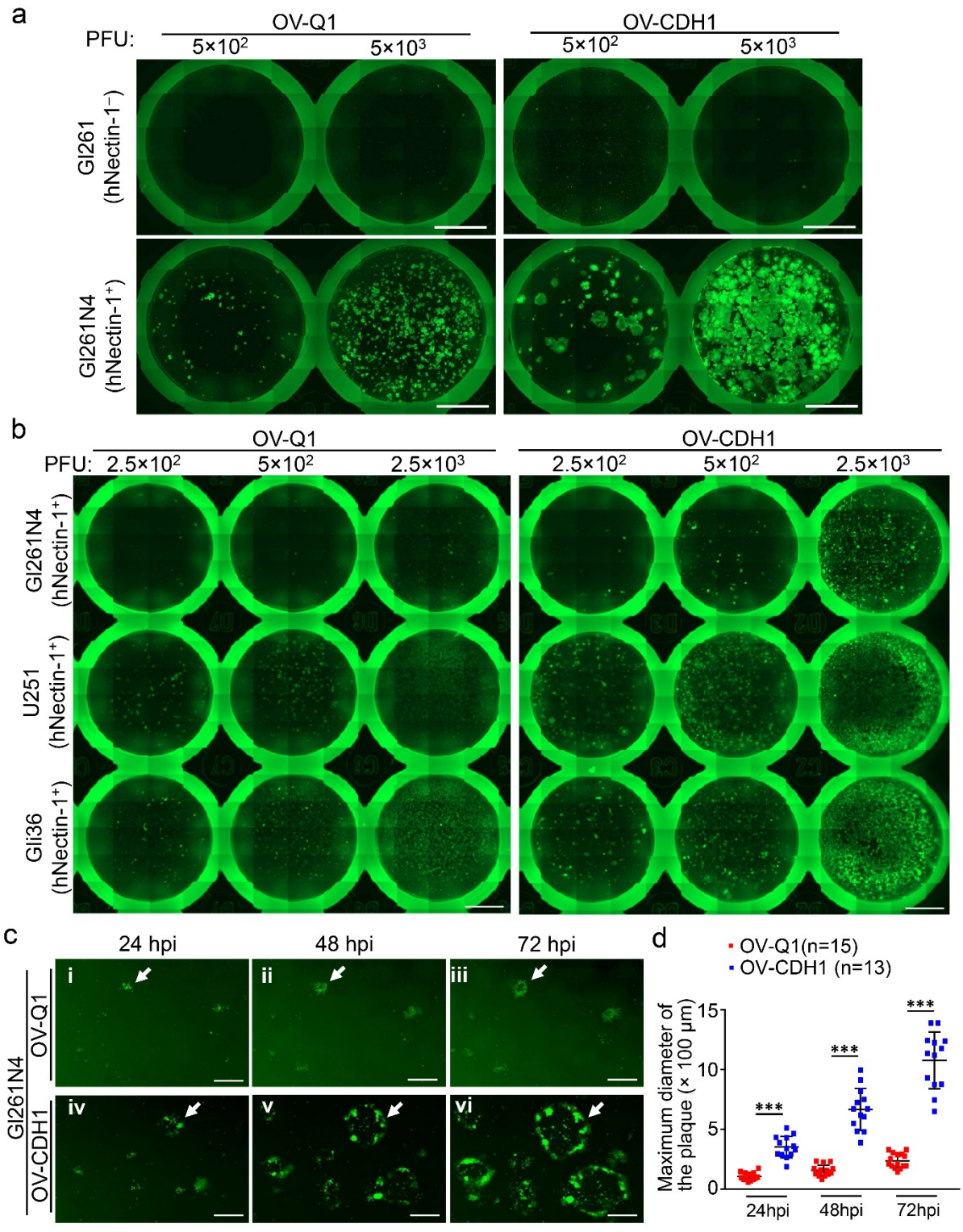

Supplementary Figure 12. Enhanced viral spread of OV-CDH1 in Gl261N4 cells. (**a**) Gl261 and Gl261N4 cells were infected with 5×10^2 and 5×10^3 PFU of OV-Q1 or OV-CDH1. At 48 hpi, cells were imaged to detect GFP expression in virus-infected cells with a fluorescence microscope to evaluate cell susceptibility to oHSV infection. Scale bar, 5,000 μm. (**b**) Monolayer Gl261N4, U251 and Gli36 cells were infected with 2.5×10^2, 5×10^2 and 2.5×10^3 PFU of OV-Q1 or OV-CDH1. At 36 hpi, cells were imaged to detect GFP expression in virus-infected cells with a fluorescence microscope to evaluate cell susceptibility to oHSV infection. Scale bar, 5,000 μm.

Experiments in (**a**) and (**b**) were repeated twice and similar data were obtained. **(c)** Monolayer Gl261N4 cells were infected with OV-Q1 or OV-CDH1 at a MOI of 0.05. At 24, 48 and 72 hpi, cells were imaged for GFP expression in virus-infected cells with a microscope. Each row shows the same view field at different time points. The white arrows in each row indicate the same plaque. Scale bar, 500 μm. (**d**) Plaque sizes from (**c**) were measured from 3 randomly selected view fields in different groups. Data are presented as mean ± SD (***$P < 0.001$). *P* values were generated by unpaired two-tailed *t*-test. Sample sizes are indicated in the figures. This experiment was repeated 3 times with similar results.

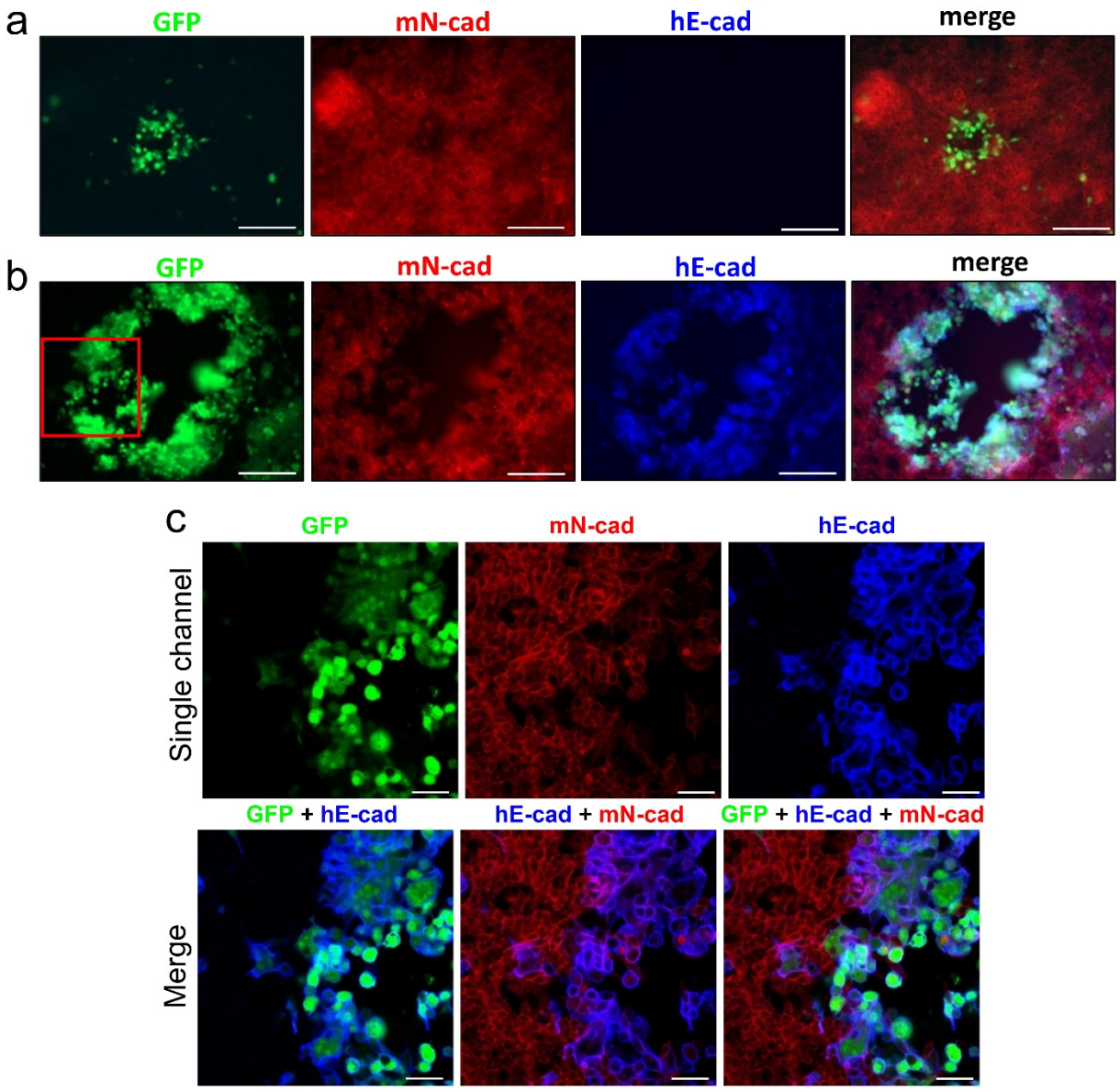

Supplementary Figure 13. Co-localization of human E-cad and murine N-cad in OV-CDH1-infected murine GBM cells. (**a,b**) Gl261N4 cells were infected with OV-Q1 (**a**) or OV-CDH1 (**b**), followed by immunofluorescence staining of the infected cells using anti-E-cad and anti-N-cad antibodies at 48 hpi. Cells were then imaged using a microscope. The images were taken using a high resolution confocal microscope. Scale bar, 150 μm. (**c**) Images of the red square indicate the vision in (b) with a higher magnification. Scale bar, 50 μm. The experiments were repeated 5 times with similar results.

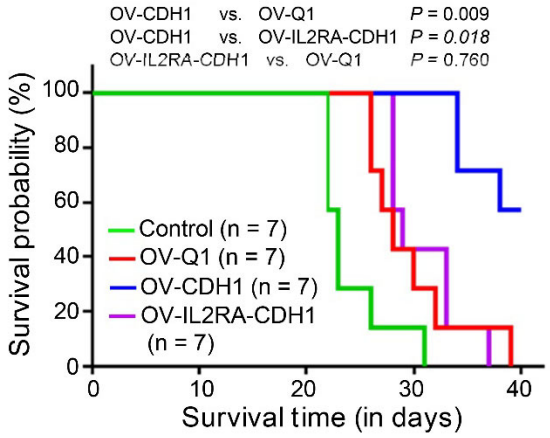

Supplementary Figure 14. Survival curves of Gl261N4-bearing mice treated with or without OV-Q1, OV-CDH1 or OV-IL2RA-CDH1. Mice were intracranially injected with 1×10^5 GL261N4 cells. 5 days after tumor implantation, mice were treated with OV-Q1, OV-CDH1 or OV-IL2RA-CDH1 at the dose of 2×10^5 PFU through intratumoral injection. Two-sided log rank test was used for statistical analysis. *P* values and sample sizes are indicated in the figure.

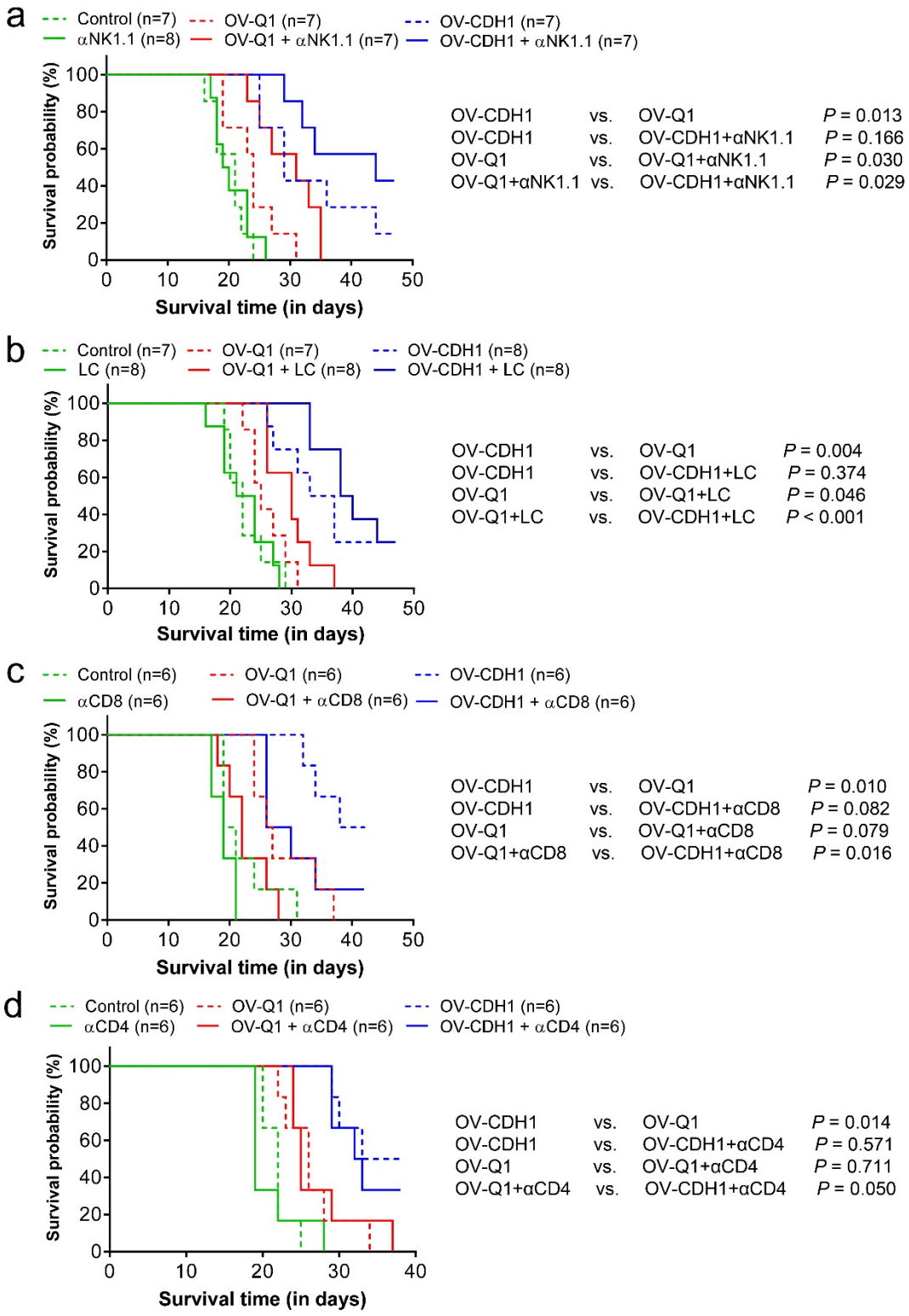

Supplementary Figure 15. The contribution of immune cells to OV-CDH1 GBM therapy. (**a**) Survival of Gl261N4 tumor-bearing C57BL/6 immunocompetent mice treated with vehicle control, OV-Q1, or OV-CDH1 after NK cell depletion. The hazard ratio of OV-CDH1 to OV-Q1 in the presence vs. absence of NK cells is 0.17 vs. 0.32. (**b**) Survival of Gl261N4 tumor-bearing C57BL/6 immunocompetent mice treated with vehicle control, OV-Q1, or OV-CDH1 after macrophage depletion. (**c**) Survival of Gl261N4 tumor-bearing C57BL/6 immunocompetent

mice treated with vehicle control, OV-Q1, or OV-CDH1 after $CD8^+$ T cell depletion. (**d**) Survival of Gl261N4 tumor-bearing C57BL/6 immunocompetent mice treated with vehicle control, OV-Q1, or OV-CDH1 after $CD4^+$ T cell depletion. Sample sizes are indicated in the figures (a-d). Two-sided log rank test was used to compare survival functions. Sample sizes and *P* values are presented in the figures.

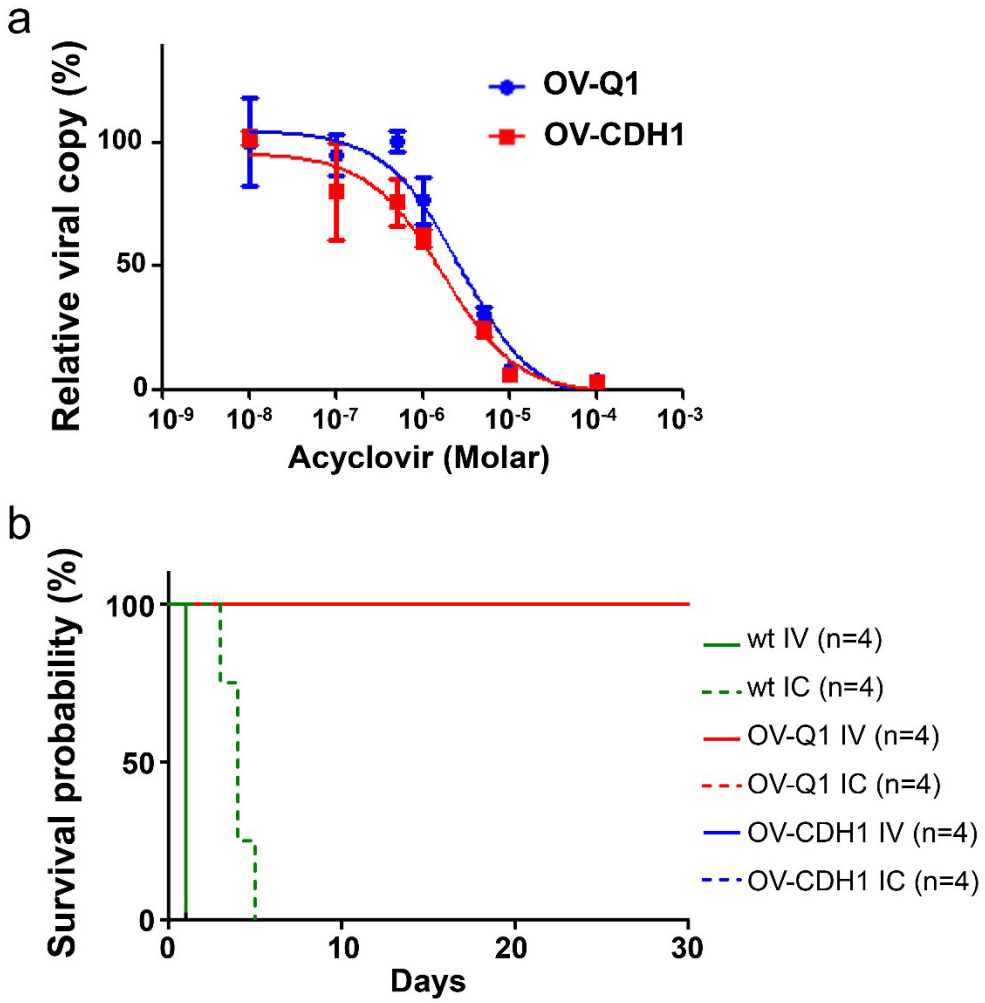

Supplementary Figure 16. Safety test for OV-CDH1. (**a**) Gli36 cells were infected with OV-Q1 or OV-CDH1 at a MOI of 5. Two hours after infection, infection media were replaced with fresh media with an increment of acyclovir concentrations. Forty-eight hours after infection, cells were harvested for DNA extraction. The HSV-1 genome copy numbers in OV-Q1 or OV-CDH1-infected cells were measured by real-time PCR with primers and a probe against gD. Data are presented as mean ± SD. The copy number vs. dose curves were established to evaluate the inhibitory effect of acyclovir against oHSV replication (n = 3 technical replicates). This experiment was repeated 3 times with similar results. (**b**) Survival curves of BLAB/c mice treated with wild-type HSV-1 (F strain), OV-Q1 or OV-CDH1 at the dose of 1×10^6 via i.c. or i.v injections (n = 4 animals). Mice injected with wild-type HSV-1 survived for no more than 5 days, while all mice treated with OV-Q1 or OV-CDH1 survived to the end of the 4-week study. The solid and dashed red lines as well as the solid and dashed blue lines overlay each other because all represent the rate of 100% survival.

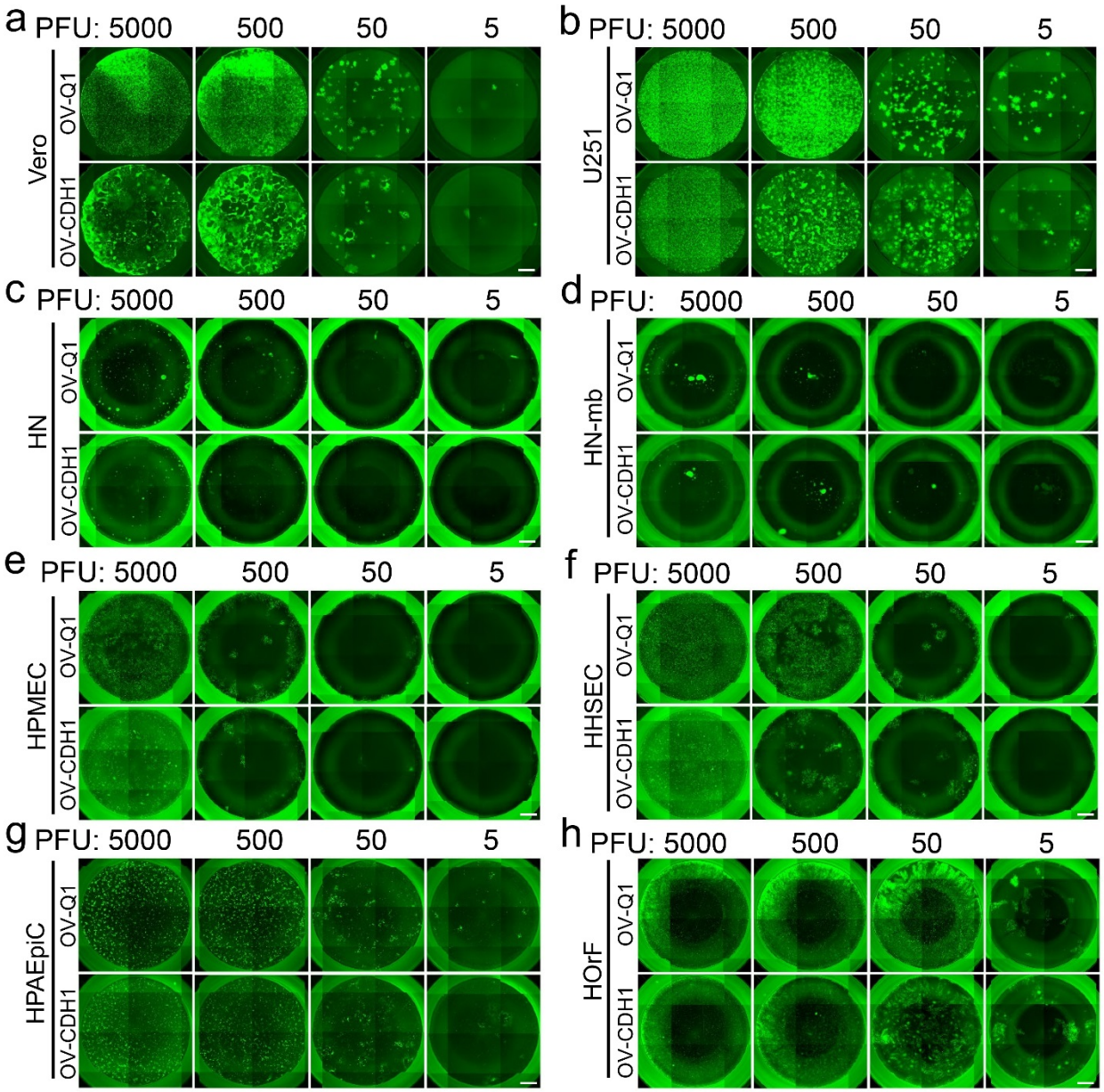

Supplementary Figure 17. Tropism of OV-CDH1. Plaque forming assays were performed with 6 different types of human primary cells including oral fibroblasts (HOrF), pulmonary microvascular endothelial cells (HPMEC), hepatic sinusoidal endothelial cells (HHSEC), pulmonary alveolar epithelial cells (HPAEpiC), neurons (HN) and neurons-midbrain (HN-mb). Vero and U251 cells were included as control. Cells were imaged under a microscope at 48 hpi. Scale bar, 1,000 μm. The experiment was repeated twice with similar results.

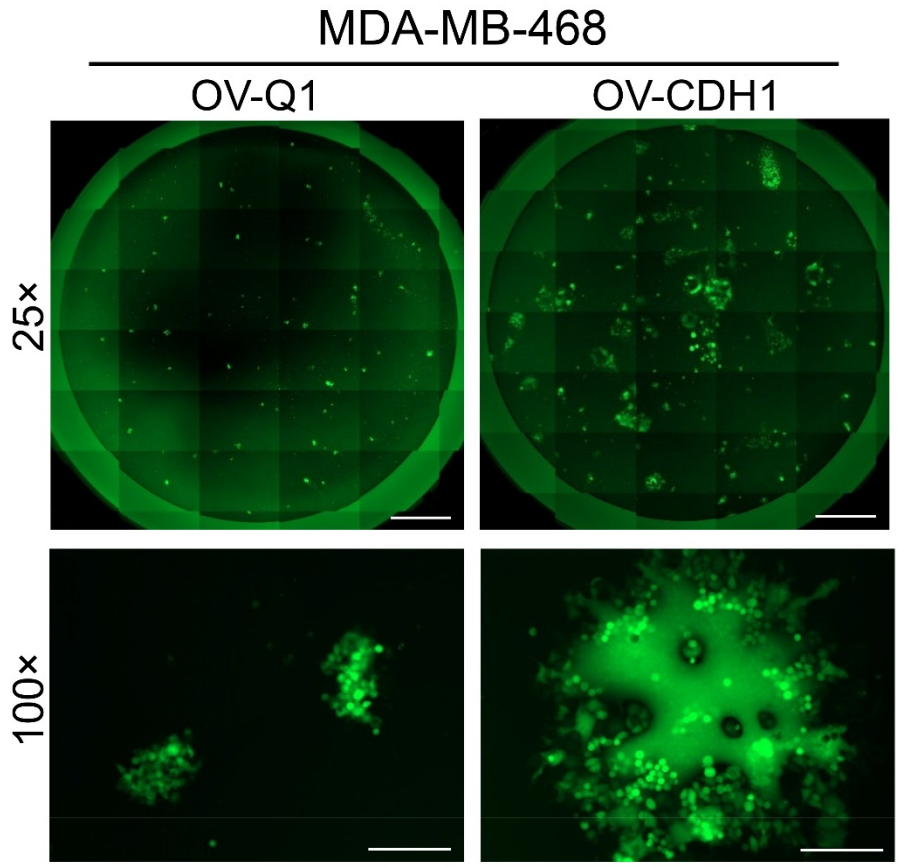

Supplementary Figure 18. Viral spread enhancement during OV-CDH1 infection among breast cancer cells. Monolayer MDA-MB-468 breast cancer cells were infected with OV-Q1 or OV-CDH1 at a MOI of 0.005. At 48 hpi, the cells were imaged to detect GFP expression in virus-infected cells via a microscopy. Scale bar, top 2,500 μm; bottom 150 μm. This experiment was repeated twice with similar results.

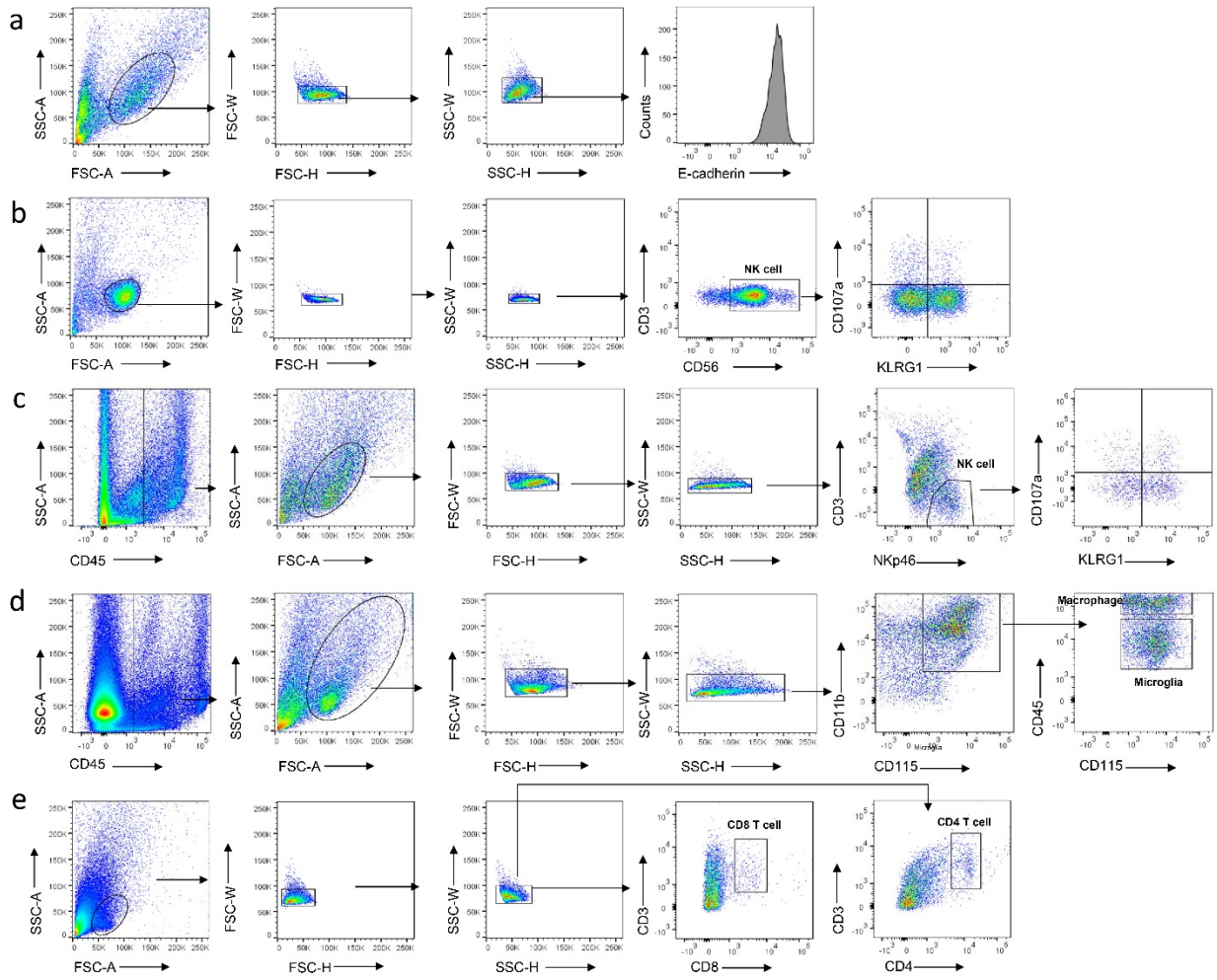

Supplementary Figure 19. Flow cytometry gating strategy. (a) To determine E-cad expression in GBM cells, live cells were further gated on FSC-A/SSC-A, FSC-H/FSC-W, and then SSC-H/SSC-W events to check surface expression levels of E-cad (for Supplementary Fig. 1d, e). (**b**) To check surface expression levels of CD107a in enriched human KLRG1^{+} and KLRG1^{-} NK cell subsets, live cells were gated on FSC-A/SSC-A, FSC-H/FSC-W, and then SSC-H/SSC-W events. NK cells were defined as CD56^{+}CD3^{-} (for Fig. 1c, d). (**c** to **e**) For flow cytometric assays on murine immune cells, live cells were gated on FSC-A/SSC-A, FSC-H/FSC-W, and then SSC-H/SSC-W. NK cells were defined as NKp46^{+}CD3^{-}; CD107a expression of NK cells are displayed in a KLRG1 vs. CD107a scatter plot (**c,** for Fig. 5c, d). Macrophages and microglia were defined as CD45^{high}CD11b^{+}CD115^{+} and CD45^{low}CD11b^{+}CD115^{+}, respectively (**d,** for Fig. 5b, h). CD4^{+} T cells were defined as CD3^{+}CD4^{+}; CD8^{+} T cells were defined as CD3^{+}CD8^{+} (**e,** for Fig. 5j, k).

Table 1. Virus distribution at 2 days after i.v. injection

	Virus distribution					
	Heart	Liver	Spleen	lung	Kidney	Brain
OV-Q1	-	++	-	+	+	-
OV-CDH1	-	++	-	+	+	-

Supplementary Table 1. Virus distribution of OV-Q1 and OV-CDH1 in BALB/c mice 2 days after i.v. injection. BALB/c mice were i.v. injected with OV-Q1 or OV-CDH1 at the dose of 1×10^6 PFU. Heart, liver, spleen, lung, kidney and brain from experimental mice were harvested 2 days after viral injection to study the distribution of the virus ($n = 3$ animals). IHC assays were performed with an anti-HSV antibody to show the distribution of OV-Q1 and OV-CDH1. "–" indicates undetectable; "+" indicates positive staining cells lower than 10%. "++" indicates positive staining cells higher than 10%.